Open Access Article. Published on 04 January 2024. Downloaded on 5/30/2026 3:01:36 AM.
This article is licensed under a Creative Commons Attribution-NonCommercial 3.0 Unported Licence.

PCCP

ROYAL SOCIETY OF CHEMISTRY

PAPER

View Article Online
View Journal | View Issue

Check for updates

Cite this: *Phys. Chem. Chem. Phys.*, 2024, **26**, 4607

Deciphering the photophysical properties of naphthalimide derivatives using ultrafast spectroscopy†

Wei Zhang,[a] Yalei Ma,[b] Hongwei Song,[c] Rong Miao,*[b] Jie Kong*[a] and Meng Zhou*[a]

Received 21st November 2023,
Accepted 3rd January 2024

DOI: 10.1039/d3cp05654f

rsc.li/pccp

Naphthalimide derivatives composed of donor–acceptor type structures hold significant promise across a wide range of applications. Here, the solvent polarity and viscosity controlled excited-state dynamics of a naphthalimide derivative with a donor–acceptor structure were studied using multiple spectroscopic techniques. From the stationary spectroscopic investigations, large Stokes shift and low fluorescence quantum yield were observed with increasing the solvent polarity, suggesting a more polar excited state relative to the ground state, which is evidenced by the Lippert–Mataga relationship. We also observe an enhanced fluorescence with a prolonged lifetime in a more viscous solution due to the restriction of excited-state molecular rearrangement. These observations result from the emerged twisted intramolecular charge transfer (TICT) state. The ultrafast spectroscopy studies further unravel a solvent polarity dependent excited state evolution from the intramolecular charge transfer state to the TICT state, revealing that the TICT state can be populated only in strong polar solvents. Control experiments by tuning the solvent viscosity in ultrafast experiments were employed to verify the excited state molecular rearrangement subsequently. These observations collectively emphasize how fine-tuning the photophysical properties of naphthalimide derivatives can be achieved through strategic manipulation of solvent polarity and viscosity.

Introduction

Organic functional molecules that consist of electron-donor (D) and -acceptor (A) moieties have attracted wide attention in the past few decades because of their potential applications in organic light emitting diodes, aggregation induced emission materials, organic photovoltaics, fluorescent probes,[1–11] *etc.* Normally, the molecules consisting of D and A subunits exhibit intramolecular charge transfer (ICT) characteristics, which can be easily modulated by the environmental polarity, viscosity, and D/A variations.[12–14] The pump-initiated excited-state conformation relaxes to a new state characterized by the conformational change entailing twisted or planar intramolecular charge transfer (TICT/PICT) when there is an intramolecular rotation.[14–23] The excited-state conformational change can thus in turn determine the unique photophysical and photochemical properties.[24]

Naphthalimide is considered as one of the most important building blocks for efficient fluorescent materials owing to its unique photophysical properties, including high electron affinity, oxidation stability, good thermal stability, and biocompatibility,[7,14,25–30] which have been explored extensively. These advantages make naphthalimide derivatives good candidates for biosensors, fluorescent cell imaging agents, and optoelectronic devices. Besides, the naphthalimide core is an electron acceptor in nature with redox potential of −1.8 V (*vs.* Ag/Ag$^+$),[31] and many of the above-mentioned applications cover the functionalization of naphthalimide with different electron-donor moieties to have the ICT character with marked solvatochromic effect.[14,30,32–34] Thus, the local environment, such as solvent polarity and viscosity, plays a crucial role in modulating the excited-state behavior of such D–A type naphthalimide derivatives because a significant dipole moment enhancement in the excited state is obtained upon photon excitation.[35–37] Previous research by Kubinyi *et al.* proposed a two state model, corresponding to the ICT and TICT, to describe the excited state

---

[a] *Hefei National Research Center for Physical Sciences at the Microscale, University of Science and Technology of China, Anhui 230026, China. E-mail: kongjie2021@ustc.edu.cn, mzhou88@ustc.edu.cn*

[b] *Laboratory of Applied Surface and Colloids Chemistry, Ministry of Education, School of Chemistry and Chemical Engineering, Shaanxi Normal University, Xi'an 710062, P. R. China. E-mail: miaorong2015@snnu.edu.cn*

[c] *Department of Chemistry–Angstrom Laboratory, Uppsala University, Box 523, Uppsala 75120, Sweden*

† Electronic supplementary information (ESI) available. See DOI: **https://doi.org/10.1039/d3cp05654f**

Open Access Article. Published on 04 January 2024. Downloaded on 5/30/2026 3:01:36 AM. This article is licensed under a Creative Commons Attribution-NonCommercial 3.0 Unported Licence.

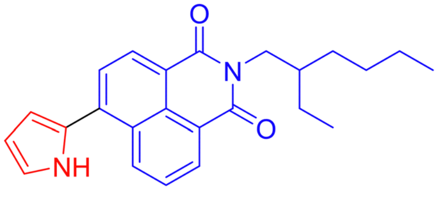

HP-NAP

Scheme 1 The molecular structure of HP-NAP.

dynamics of naphthalimide derivatives by applying theoretical calculations, stationary and time-resolved fluorescence spectra, whereas direct visual evidence of the conversion from ICT to TICT is absent.[32] Therefore, investigating the photophysical properties of the long-term studied naphthalimide derivatives will be conducive to designing high-performance molecules with ICT character.

In this work, we report a comprehensive investigation of a naphthalimide derivative, 2-(2-ethylhexyl)-6-(1*H*-pyrrol-2-yl)-1*H*-benzo[de]isoquinoline-1,3(2*H*)-dione (HP-NAP, the molecular structure is shown in Scheme 1),[8] that is composed of electron-acceptor naphthalimide and electron-donor pyrrole. We found that the Stokes shifts and fluorescence quantum yields of HP-NAP are sensitive to the environmental polarity, and viscosity-dependent measurements suggest that restricting molecular rotation is beneficial for obtaining stronger fluorescence intensity and longer lifetime. Ultrafast spectroscopy provides the main insights and allows visualization of the dynamic process of ICT converting to the TICT state, which is governed by the environmental polarity and viscosity. These results are important for deeply understanding the photophysical properties of naphthalimide derivatives.

Materials and methods

Materials

The synthesis and characterization of HP-NAP were reported previously.[8] All solvents used in this work, including hexane (Hex), dichloromethane (CH_2Cl_2), tetrahydrofuran (THF), acetonitrile (ACN), and cyclohexane (CHX), were purchased from Sinopharm Chemical Reagent Co., Ltd, and all solvents were used without further purification. 9,10-Diphenylanthracene (9,10-DPA) and polymethyl methacrylate (PMMA) were purchased from Sinopharm Chemical Reagent Co., Ltd and Shanghai Macklin Biochemical Technology Co., Ltd, respectively.

Quantum chemical calculations

Theoretical calculations were performed based on density functional theory (DFT) and time-dependent DFT (TD-DFT) by employing the Gaussian 16, Revision A.03 package.[38] Optimization of the ground state geometry was obtained using the B3LYP[39] functional at the basis set 6-311G** level. The alkyl chain on the N-atom is reduced to a methyl group for calculation simplicity.

Stationary spectroscopy

The steady-state spectra (including UV-vis absorption and fluorescence spectra) were collected using Agilent Cary 60 UV-Vis and Agilent Cary Eclipse fluorescence spectrometers, respectively. The fluorescence quantum yields were measured using a comparative method, where the reference is a solution of 9,10-DPA in CHX solvent ($\Phi_f = 0.955$, excited at 366 nm).[40] The stationary data was obtained with sample concentrations of 10^{-5} M.

Fluorescence lifetime and ultrafast spectroscopy measurements

The fluorescence lifetime was acquired on a time-correlated single photon counting spectrometer (FluoTime 300, PicoQuant, Germany) under 375 nm picosecond laser (PDL 820, PicoQuant diode laser) excitation.

The femtosecond transient absorption (fs-TA) spectroscopy measurements were performed on a home-built pump–probe set-up. The laser pulse (800 nm, 35 fs pulse width, 1 kHz repetition rate) was generated by a regeneratively amplified Ti:sapphire laser (Coherent Astrella-Tunalbe-USP, USA). The output of the pulse is divided into two beams with a beam splitter. The 400 nm pump beam was produced by doubling the 800 nm pulse with a beta barium borate crystal (type I, 0.5 mm thickness); the power of the pump pulse was set as 0.1 μJ. The probe pulse was delayed by a computer-controlled optical delay line and then focused on a thin sapphire plate to generate the white light supercontinuum, which split into two beams by using a broadband 50/50 beam splitter as the signal and reference beams (450–800 nm). The focused pump and probe pulses overlapped into a sample cuvette. The mutual polarization between the pump and probe pulses was set to 54.7° by placing a half-wave plate in the pump beam. The solution concentrations were set to around 10^{-5} M, and there was no photodegradation after fs-TA experiments by checking the stationary absorption spectra.

Results and discussion

Optimized ground state (S_0) geometry and charge density distribution on frontier molecular orbitals (FMOs) of HP-NAP are depicted in Fig. 1a–c. The highest occupied molecular orbital (HOMO) comprises the charge distribution between the naphthalimide and pyrrole moieties, while the charge density on the lowest unoccupied molecular orbital (LUMO) is mainly localized on the naphthalimide core, making the vertical transition a local excited (LE) dominated character. More discussion about the theoretically calculated excited state (S_1) of HP-NAP, as well as a short comment, can be found in the S1 part of the ESI.†

Fig. 1d shows the stationary absorption and fluorescence spectra of HP-NAP in different polar solvents. These solvent polarity-independent absorption bands with well-resolved vibronic peaks at ∼345 nm can be ascribed to the LE transition. In terms of the lower-energy absorption bands centered at

Open Access Article. Published on 04 January 2024. Downloaded on 5/30/2026 3:01:36 AM.
This article is licensed under a Creative Commons Attribution-NonCommercial 3.0 Unported Licence.

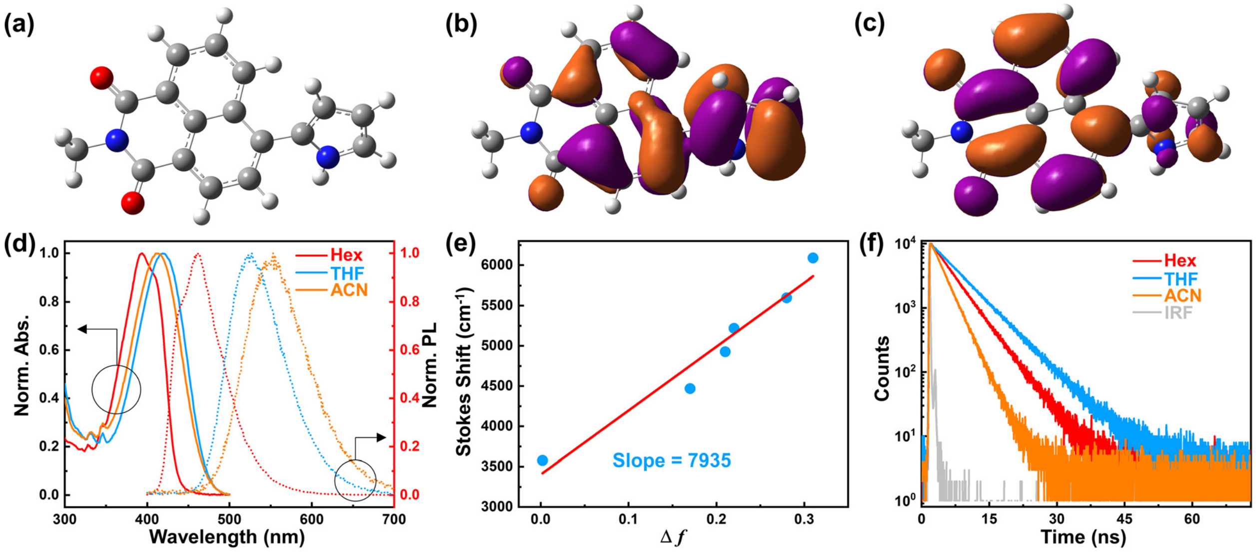

Fig. 1 (a) The optimized geometry of HP-NAP at the S_0 state. The (b) HOMO and (c) LUMO of HP-NAP at the optimized S_0 geometry. (d) The normalized stationary absorption and fluorescence spectra of HP-NAP in different solvents. (e) Stokes shifts of HP-NAP relative to the solvent orientation polarizability. (f) The fluorescence decay profiles of HP-NAP in different solvents.

~400 nm, the marginal solvatochromic shifts are observed, accounting for the LE dominated vertical transition from S_0 to S_1. This is also evidenced by the shoulder peak at ~400 nm in Hex that collaborates with the absorption bands in THF and ACN. In contrast, the fluorescence spectra show a significant red shift with an enhancement of dielectric environment, where we observe the structured band in Hex evolve into broader and Gaussian-like bands in THF and ACN. The dynamic evolution of absorption and fluorescence spectra of HP-NAP suggests the increase of the dipole moment under photon excitation, accounting for a pump-initiated S_1 state with LE character, while the relaxed S_1 state with LE character in Hex evolves into the ICT character in polar solvents.

To further clarify the ICT character caused by the dipole moment difference between the S_0 and S_1 states ($\Delta\mu_{ge}$), the Lippert–Mataga equation[41–44] is applied to evaluate the $\Delta\mu_{ge}$ by plotting the Stokes shift against the solvent orientation polarizability (Δf) as shown in Fig. 1e, the detailed data are provided in Table S1 (ESI†). The relationship between Stokes shift and Δf is as follows,

$$\Delta\nu = \nu_{abs} - \nu_{em} = \frac{1}{4\pi\varepsilon_0}\frac{2\Delta f}{hca^3}(\Delta\mu_{ge})^2 + \text{const} \quad (1)$$

$$\Delta f = \frac{\varepsilon - 1}{2\varepsilon + 1} - \frac{n^2 - 1}{2n^2 + 1} \quad (2)$$

Table 1 The photophysical data of HP-NAP in different solvents

Solvent	Abs/nm	Em/nm	Stokes shift/cm^{-1}	τ/ns	Φ	k_r/ns^{-1}	k_{nr}/ns^{-1}
Hex	395	460	3577	3.36	1.00	0.30	0.00
THF	419	528	4927	6.11	0.54	0.09	0.08
ACN	412	550	6090	2.69	0.18	0.07	0.31

where the $\Delta\nu$ is the Stokes shift, the ν_{abs} and ν_{em} are the wavenumbers of the absorption and emission peaks, respectively, c is the speed of light in a vacuum, ε_0 is the vacuum permittivity, h is Planck's constant, a is the Onsager cavity radius, and the ε and n are the dielectric constant and refractive index of the solvents, respectively. The Onsager cavity radius of HP-NAP is 4.98 Å as determined by the DFT calculation. From the slope of the plot, the $\Delta\mu_{ge}$ of HP-NAP is determined to be 10 D. Based on the theoretical calculated dipole moment in the S_0 state (5 D), the obtained S_1 value (15 D) is three times enhanced relative to the S_0 value, showing a strong charge transfer character of HP-NAP.

The fluorescence quantum yields and lifetime (Fig. 1f) were also measured, and the radiative and nonradiative rate constants were calculated by the following equations:

$$k_r = \Phi/\tau \quad (3)$$

$$1/\tau = k_r + k_{nr} \quad (4)$$

where the Φ is the fluorescence quantum yield, τ is the fluorescence lifetime, and k_r and k_{nr} are the radiative and nonradiative rate constants, respectively. The obtained photophysical data are summarized in Table 1. The pronounced fluorescence spectral shift is accompanied by the significant change in fluorescence quantum yields, where almost 100% of the quantum yield in Hex drops to 54% in THF. In the meantime, the slight increase of solvent polarity induces the elongation of the fluorescence lifetime from 3.36 ns in Hex to 6.11 ns in THF. Further enhancing the dielectric constant of the solvent leads to the decrease of the quantum yield (18%) and lifetime (2.69 ns) in ACN simultaneously. We suggest that the obtained photophysical data of HP-NAP arises from the competition between the LE/ICT state and TICT state, where the LE state dominates the deactivation process in Hex while TICT is the

Open Access Article. Published on 04 January 2024. Downloaded on 5/30/2026 3:01:36 AM.
This article is licensed under a Creative Commons Attribution-NonCommercial 3.0 Unported Licence.

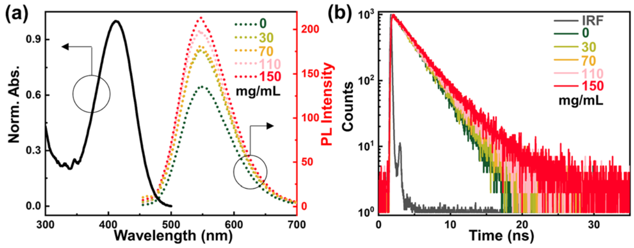

Fig. 2 The viscosity-dependent measurements of HP-NAP in the ACN solvent dissolved with different mass concentrations of PMMA. The viscosity-dependent (a) absorption and fluorescence spectra and (b) fluorescence decay profiles of HP-NAP.

prominent property in ACN, and there is an equilibrium between ICT and TICT in THF. To distinguish the twisting-oriented properties in polar solvent ACN, we further conducted the measurements in ACN solvent that dissolved with PMMA to perform the viscosity-dependent experiments.

The viscosity-dependent measurements of HP-NAP are shown in Fig. 2, where the different mass concentrations of PMMA are used to provide a conformational change limiting environment. It is found that the increased concentration of PMMA results in fluorescence enhancement (Fig. 2a), and one can observe a gradual blue-shift of fluorescence spectra (Fig. S2a, ESI†). To show a clearer presentation of the PMMA concentration controlled blueshift of the fluorescence spectra, the differential spectrum between the normalized fluorescence spectra with PMMA concentration of 150 mg mL^{-1} and of 0 mg mL^{-1} is provided in Fig. S2b (ESI†), where the positive signal at the blue side (∼ 515 nm) clearly shows the blueshift of the fluorescence spectrum at a PMMA concentration of 150 mg mL^{-1} relative to that of 0 mg mL^{-1}. In addition, it is also noted that the increase of the viscosity can boost the fluorescence lifetime (Fig. 2b and Table S2, ESI†). These results should be considered as an outcome of restricting the nonradiative decay channel that enhances the fluorescence, while restricting the excited-state bond rotation will blue-shift the fluorescence.

So far, it is evident that the excited state relaxation pathways of HP-NAP are strongly dependent on the environment polarity and viscosity. The efficient nonradiative decay channel and pronounced decrease of fluorescence quantum yield upon enhancement of solvent polarity correlate well with the relatively stronger excited-state dipole moment μ_e. The longer fluorescence lifetime, and stronger and blue-shifted fluorescence with increasing solvent viscosity result from the suppression of excited-state conformation change process. To gain a deeper understanding of the excited state dynamics of HP-NAP, we then performed fs-TA spectroscopy under different dielectric constant conditions.

The obtained fs-TA data (Fig. 3) in different polar solvents illustrate the competition between the electronic excited states upon photon excitation at the lowest absorption band (400 nm). The initial recorded spectra of HP-NAP in nonpolar solvent Hex consist of a negative peak centered at 450 nm and a broad positive band across from 475 nm to 750 nm with several absorption peaks (Fig. 3(a) and (b)). The former negative peak can be ascribed to the stimulated emission (SE) by comparing it with the stationary fluorescence spectrum in Hex (Fig. 1d), confirming that the pump-populated state is a LE state; the latter positive peaks are the excited state absorption (ESA) from S_1 to the higher singlet excited states. No pronounced dielectric-controlled dynamics is observed during the detection window. In the medium polar THF, the dynamic spectral evolution is different. The initial fs-TA spectrum of HP-NAP in THF is different from that in Hex, as the initial SE signal in THF is located at ∼525 nm, which can be ascribed to the ICT signal compared to the stationary fluorescence spectrum in Fig. 1d. This is because of the strong solvation effect making a quick transformation from LE to ICT, which cannot be captured in our fs-TA set-up. As the time delay continues, the band

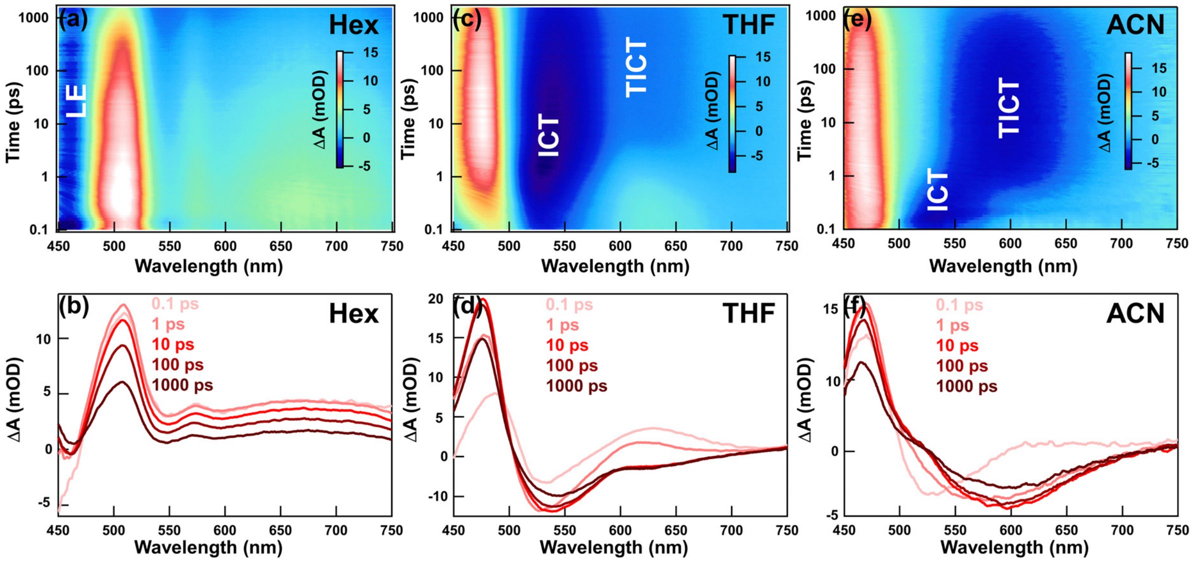

Fig. 3 The fs-TA maps (up panel) and spectra (low panel) of HP-NAP in different polar solvents.

Open Access Article. Published on 04 January 2024. Downloaded on 5/30/2026 3:01:36 AM.
This article is licensed under a Creative Commons Attribution-NonCommercial 3.0 Unported Licence.

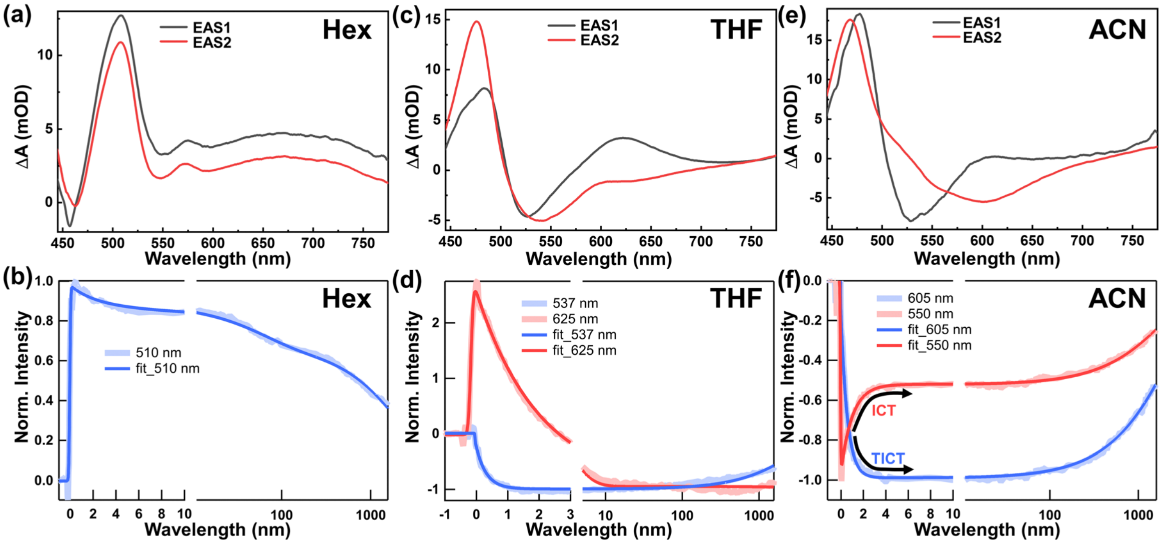

Fig. 4 The global analysis results (up panel) and representative kinetics (low panel) of HP-NAP in different polar solvents.

at 525 nm shows a slight red shift and intensity decrease, which is accompanied by the generation of a new SE band at 625 nm. This spectral evolution is attributed to the excited-state conversion from the ICT to TICT state. However, we should highlight that the SE intensity at 525 nm is stronger than the newly formed SE signal at 625 nm from the initial time to the end time. The spectral evolution in ACN shows a faster TICT generation than in THF because a stronger dielectric environment accelerates the conversion from ICT to TICT, and the ICT SE signal disappears within ∼1 ps (Fig. 3e).

To reveal the relaxation mechanism, the global analysis[45] was conducted to extract the transient species. Fig. 4 shows the evolution-associated spectra (EAS) and the representative kinetics at the characteristic wavelengths, and the detailed fitting data is displayed in Table S3 (ESI†). It is obvious that there is no new transient species generated in Hex, and two EAS are obtained by global analysis (Fig. 4a), corresponding to LE and vibrational cooling LE (LE'). Being in such a regime, the vibrational cooling process of excited state species toward ambient temperature leads to band narrowing (Fig. S3a, ESI†),[46,47] *i.e.*, the band narrowing process is due to the vibrational cooling (Fig. S3b, ESI†). For HP-NAP in THF, the first transient component (EAS1) extracted from the fs-TA data is the ICT state, whose spectral profile is similar to the initial spectral profile from fs-TA data (Fig. 3d). While the second transient component contains two SE signals which belong to the ICT and TICT states, thus we assign the EAS2 to the equilibrium state between the ICT and TICT. This is also confirmed by the kinetic comparison in Fig. 4d, which shows that though the kinetic traces at 625 nm exhibit the generation of the TICT state, there is no obvious intensity decrease of the ICT state even at 300 ps. Then we turn our attention to HP-NAP in ACN, and there is an isosbestic point located at ∼560 nm (Fig. 3f), suggesting the state-state conversion process and that the fs-TA can be well decomposed into two species (Fig. 4e), corresponding to the ICT and TICT states. The kinetic traces shown in Fig. 4f disclose that the decay of the ICT state (505 nm) generates the TICT state (605 nm) rather than the S_0 state. One could argue that the TICT signals in THF (625 nm) and ACN (605 nm) are not at the same position because the ICT signal in THF (525 nm) is always much stronger than the TICT signal, which shifts the TICT signal to a red position. Compared

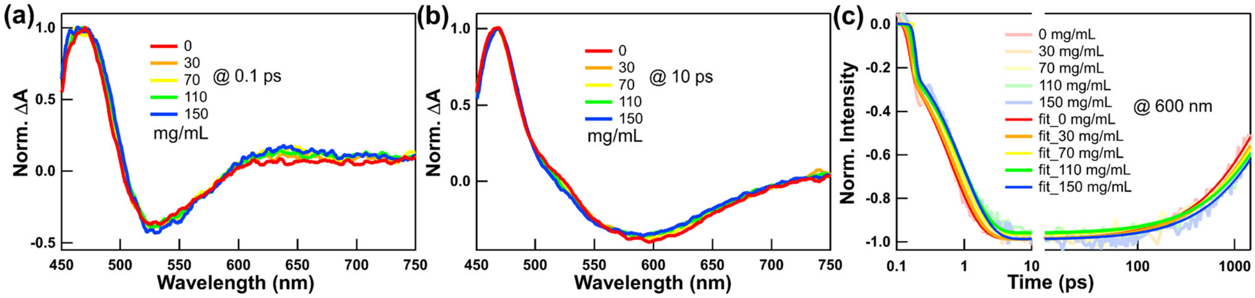

Fig. 5 The viscosity-dependent fs-TA spectra of HP-NAP in ACN solvents that dissolved different mass concentrations of PMMA. The normalized fs-TA spectra at a time delay of (a) 0.1 ps and (b) 10 ps, and (c) the normalized viscosity-dependent kinetics comparison at 600 nm.

Open Access Article. Published on 04 January 2024. Downloaded on 5/30/2026 3:01:36 AM.
This article is licensed under a Creative Commons Attribution-NonCommercial 3.0 Unported Licence.

with previous literature,[14] the equilibrium state between the ICT and TICT of the naphthalimide derivative is firstly reported in our work.

The observed changes in fs-TA spectra in ACN are attributed to the population conversion from ICT to TICT accompanied by the excited-state molecular rearrangement from a quasi-planar structure to a perpendicular conformation as we discussed above. To verify the excited state molecular rearrangement, we conducted the viscosity-dependent fs-TA measurements of HP-NAP (Fig. 5). At the initial time delay of 0.1 ps, the SE signals that belong to the ICT state are almost the same for all samples; while we observe gradual blue shifted SE signals at a time delay of 10 ps (Fig. 5b) with an increase in the solvent viscosity, which is due to the limited molecular rearrangement environment. The TA differential spectrum at a time delay of 10 ps between the spectra with PMMA concentration of 150 mg $\mathrm{mL^{-1}}$ and PMMA concentration of 0 mg $\mathrm{mL^{-1}}$ is also provided in Fig. S4 (ESI†), the negative signal at 520 nm (at the SE region) confirms the blueshift of the SE signal upon increasing the solvent viscosity. In addition, the kinetic trace comparison at 600 nm (Fig. 5c) shows a slower generation and slower relaxation of the TICT state with 150 mg $\mathrm{mL^{-1}}$ PMMA in ACN, further verifying that the high viscosity environment can limit the excited state molecular rotation, thus slowing the generation and deactivation of TICT. The detailed fitting time constants from viscosity-dependent fs-TA spectra can be found in Table S4 (ESI†).

Based on the current results, the fs-TA measurements in Hex represent the excitation relaxation from the LE state with quasi-planar geometry, while the result from medium polar THF show a competition between the ICT and TICT state, and finally, the fs-TA data in ACN corresponds to the TICT dominated relaxation. The results from the fs-TA spectra nicely match the earlier discussion obtained from the solvent polarity- and viscosity-dependent stationary absorption and fluorescence spectra, as well as the time-resolved fluorescence experiments. As seen from Scheme 2, we provide the schematic diagram of the solvent polarity controlled excited-state relaxation pathways of HP-NAP, which presents that the dynamic solvation determines whether the TICT generates, and more polar solvent induces more pronounced fluorescence quenching.

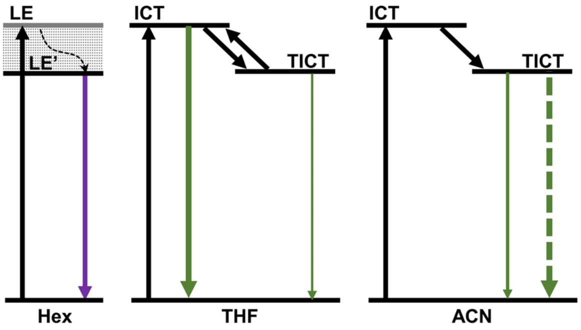

Scheme 2 The schematic diagram of the solvent polarity controlled excited-state relaxation pathways of HP-NAP.

Conclusions

In summary, the photophysical properties of naphthalimide derivative HP-NAP were thoroughly investigated by employing solvent polarity- and viscosity-dependent stationary and ultrafast spectroscopies. HP-NAP shows LE character in nonpolar Hex and a high fluorescence quantum yield (∼100%) is achieved. However, an increase in solvent polarity gives rise to the formation of the TICT state, and efficient nonradiative pathways are enabled, which strongly quenched the fluorescence. The fs-TA spectra confirm the results from stationary measurements and reveal the detailed excited-state evolution pathways: the vibrational cooling process from the pump-initiated LE state in Hex, the competition of ICT and TICT in THF, and the TICT-oriented relaxation in ACN. Furthermore, the viscosity-controlled experiments of similar polarity with ACN show enhancement of fluorescence as viscosity increases, as well as a blue-shifted SE signal and slower generation of the TICT state, confirming the excited state molecular rotation process. These results are helpful for understanding the photophysics of naphthalimide derivatives.

Conflicts of interest

There are no conflicts to declare.

Acknowledgements

This work was supported by NSFC (22203085) and Chinese Academy of Sciences (YSBR-007).

References

1 J. Kong, W. Zhang, X. Zhang, B. Liu, Y. Li and A. Xia, *J. Chem. Phys.*, 2022, **156**, 174902.
2 G. Zhang, F. R. Lin, F. Qi, T. Heumüller, A. Distler, H.-J. Egelhaaf, N. Li, P. C. Y. Chow, C. J. Brabec, A. K. Y. Jen and H.-L. Yip, *Chem. Rev.*, 2022, **122**, 14180–14274.
3 Y.-Z. Shi, H. Wu, K. Wang, J. Yu, X.-M. Ou and X.-H. Zhang, *Chem. Sci.*, 2022, **13**, 3625–3651.
4 Y.-K. Qu, Q. Zheng, J. Fan, L.-S. Liao and Z.-Q. Jiang, *Acc. Mater. Res.*, 2021, **2**, 1261–1271.
5 M. Mamada, H. Katagiri, C.-Y. Chan, Y.-T. Lee, K. Goushi, H. Nakanotani, T. Hatakeyama and C. Adachi, *Adv. Funct. Mater.*, 2022, **32**, 2204352.
6 W. Zhang, L. Zhao, B. W. Laursen and J. Chen, *Phys. Chem. Chem. Phys.*, 2022, **24**, 26731–26737.
7 H.-Q. Dong, T.-B. Wei, X.-Q. Ma, Q.-Y. Yang, Y.-F. Zhang, Y.-J. Sun, B.-B. Shi, H. Yao, Y.-M. Zhang and Q. Lin, *J. Mater. Chem. C*, 2020, **8**, 13501–13529.
8 R. Miao, J. Li, C. Wang, X. Jiang, Y. Gao, X. Liu, D. Wang, X. Li, X. Liu and Y. Fang, *Adv. Sci.*, 2022, **9**, 2104609.
9 G. Yang, Y. Ran, Y. Wu, M. Chen, Z. Bin and J. You, *Aggregate*, 2022, **3**, e127.

Open Access Article. Published on 04 January 2024. Downloaded on 5/30/2026 3:01:36 AM. This article is licensed under a Creative Commons Attribution-NonCommercial 3.0 Unported Licence.

10 N. Masimukku, D. Gudeika, D. Volyniuk, O. Bezvikonnyi, J. Simokaitiene, V. Matulis, D. Lyakhov, V. Azovskyi and J. V. Gražulevičius, *Phys. Chem. Chem. Phys.*, 2022, **24**, 5070–5082.

11 C. Rizzo, P. Cancemi, L. Mattiello, S. Marullo and F. D'Anna, *ACS Appl. Mater. Interfaces*, 2020, **12**, 48442–48457.

12 W. Zhang, J. Kong, R. Z. An, J. Zhang, Y. Zhou, L.-S. Cui and M. Zhou, *Aggregate*, 2023, e416.

13 X. Niu, P. Gautam, Z. Kuang, C. P. Yu, Y. Guo, H. Song, Q. Guo, J. M. W. Chan and A. Xia, *Phys. Chem. Chem. Phys.*, 2019, **21**, 17323–17331.

14 J. Jovaišaitė, P. Baronas, G. Jonusauskas, D. Gudeika, A. Gruodis, J. V. Gražulevičius and S. Juršėnas, *Phys. Chem. Chem. Phys.*, 2023, **25**, 2411–2419.

15 K. Hanaoka, S. Iwaki, K. Yagi, T. Myochin, T. Ikeno, H. Ohno, E. Sasaki, T. Komatsu, T. Ueno, M. Uchigashima, T. Mikuni, K. Tainaka, S. Tahara, S. Takeuchi, T. Tahara, M. Uchiyama, T. Nagano and Y. Urano, *J. Am. Chem. Soc.*, 2022, **144**, 19778–19790.

16 C. Wang, W. Chi, Q. Qiao, D. Tan, Z. Xu and X. Liu, *Chem. Soc. Rev.*, 2021, **50**, 12656–12678.

17 R. Grotjahn, *J. Chem. Phys.*, 2023, **159**, 174102.

18 A. Iagatti, B. Patrizi, A. Basagni, A. Marcelli, A. Alessi, S. Zanardi, R. Fusco, M. Salvalaggio, L. Bussotti and P. Foggi, *Phys. Chem. Chem. Phys.*, 2017, **19**, 13604–13613.

19 A. Barak, N. Dhiman, F. Sturm, F. Rauch, Y. A. Lakshmanna, K. S. Findlay, A. Beeby, T. B. Marder and S. Umapathy, *J. Phys. Chem. C*, 2023, **127**, 5855–5865.

20 I. Knysh, I. Duchemin, X. Blase and D. Jacquemin, *J. Chem. Phys.*, 2022, **157**, 194102.

21 J. Dobkowski, J. Wójcik, W. Koźmiński, R. Kołos, J. Waluk and J. Michl, *J. Am. Chem. Soc.*, 2002, **124**, 2406–2407.

22 C. Wang, W. Jiang, D. Tan, L. Huang, J. Li, Q. Qiao, P. Yadav, X. Liu and Z. Xu, *Chem. Sci.*, 2023, **14**, 4786–4795.

23 K. Basuroy, J. d J. Velazquez-Garcia, D. Storozhuk, R. Henning, D. J. Gosztola, S. Thekku Veedu and S. Techert, *J. Chem. Phys.*, 2023, **158**, 054304.

24 Z. R. Grabowski, K. Rotkiewicz and W. Rettig, *Chem. Rev.*, 2003, **103**, 3899–4032.

25 R. Tandon, V. Luxami, N. Tandon and K. Paul, *Bioorg. Chem.*, 2022, **121**, 105677.

26 A. S. Oshchepkov, M. S. Oshchepkov, M. V. Oshchepkova, A. Al-Hamry, O. Kanoun and E. A. Kataev, *Adv. Opt. Mater.*, 2021, **9**, 2001913.

27 S. Banerjee, E. B. Veale, C. M. Phelan, S. A. Murphy, G. M. Tocci, L. J. Gillespie, D. O. Frimannsson, J. M. Kelly and T. Gunnlaugsson, *Chem. Soc. Rev.*, 2013, **42**, 1601–1618.

28 H. Yu, Y. Guo, W. Zhu, K. Havener and X. Zheng, *Coord. Chem. Rev.*, 2021, **444**, 214019.

29 X. Tian, K. Shoyama, B. Mahlmeister, F. Brust, M. Stolte and F. Würthner, *J. Am. Chem. Soc.*, 2023, **145**, 9886–9894.

30 J. R. Swartzfager, G. Chen, T. Francese, G. Galli and J. B. Asbury, *Phys. Chem. Chem. Phys.*, 2023, **25**, 3151–3159.

31 D. Gudeika, R. R. Reghu, J. V. Grazulevicius, G. Buika, J. Simokaitiene, A. Miasojedovas, S. Jursenas and V. Jankauskas, *Dyes Pigm.*, 2013, **99**, 895–902.

32 Z. Szakács, S. Rousseva, M. Bojtár, D. Hessz, I. Bitter, M. Kállay, M. Hilbers, H. Zhang and M. Kubinyi, *Phys. Chem. Chem. Phys.*, 2018, **20**, 10155–10164.

33 W. Zhang, J. Kong, R. Miao, H. Song, Y. Ma, M. Zhou and Y. Fang, *Adv. Funct. Mater.*, 2023, 2311404.

34 X. Xiao, Y. Yan, A. A. Sukhanov, S. Doria, A. Iagatti, L. Bussotti, J. Zhao, M. Di Donato and V. K. Voronkova, *J. Phys. Chem. B*, 2023, **127**, 6982–6998.

35 J. R. Lakowicz, *Principles of fluorescence spectroscopy*, Springer Science & Business Media, 2013.

36 E. W. Castner Jr, M. Maroncelli and G. R. Fleming, *J. Chem. Phys.*, 1987, **86**, 1090–1097.

37 M. L. Horng, J. A. Gardecki, A. Papazyan and M. Maroncelli, *J. Phys. Chem.*, 1995, **99**, 17311–17337.

38 M. Frisch, G. Trucks, H. Schlegel, G. Scuseria, M. Robb, J. Cheeseman, G. Scalmani, V. Barone, G. Petersson, H. Nakatsuji *et al.*, *Gaussian, Revision C.02*, Gaussian, Inc., Wallingford CT, 2019, vol. 16.

39 P. J. Stephens, F. J. Devlin, C. F. Chabalowski and M. J. Frisch, *J. Phys. Chem.*, 1994, **98**, 11623–11627.

40 A. M. Brouwer, *Pure Appl. Chem.*, 2011, **83**, 2213–2228.

41 N. Mataga, *Bull. Chem. Soc. Jpn.*, 1963, **36**, 654–662.

42 N. Mataga, Y. Kaifu and M. Koizumi, *Bull. Chem. Soc. Jpn.*, 1955, **28**, 690–691.

43 N. Mataga, Y. Kaifu and M. Koizumi, *Bull. Chem. Soc. Jpn.*, 1956, **29**, 465–470.

44 E. Lippert, *Z. Naturforschung A*, 1955, **10**, 541–545.

45 J. Snellenburg, S. Laptenok, R. Seger, K. Mullen and I. Van Stokkum, *J. Stat. Soft.*, 2012, **49**, 1–22.

46 W. Zhang, J. Kong, D. Hu, M. Tao, X. Niu, S. Vdović, D. Aumiler, Y. Ma and A. Xia, *J. Phys. Chem. C*, 2020, **124**, 5574–5582.

47 S. M. Aly, A. Usman, M. AlZayer, G. A. Hamdi, E. Alarousu and O. F. Mohammed, *J. Phys. Chem. B*, 2015, **119**, 2596–2603.